Size and mechanics effects in surface-induced melting of nanoparticles

Valery I Levitas[1] & Kamran Samani[2]

Various melting-related phenomena (like surface melting, size dependence of melting temperature, melting of few nm-size particles and overheating at a very fast heating rate) are of great fundamental and applied interest, although the corresponding theory is still lacking. Here we develop an advanced phase-field theory of melting coupled to mechanics, which resolves numerous existing contradictions and allowed us to reveal exciting features of melting problems. The necessity of introducing an unexpected concept, namely, coherent solid–melt interface with uniaxial transformation strain, is demonstrated. A crossover in temperature dependence of interface energy for radii below 20 nm is found. Surface-induced premelting and barrierless melt nucleation for nanoparticles down to 1 nm radius is studied, and the importance of advanced mechanics is demonstrated. Our model describes well experimental data on the width of the molten layer versus temperature for the Al plane surface and on melting temperature versus particle radius.

[1] Departments of Aerospace Engineering, Mechanical Engineering and Material Science and Engineering, Iowa State University, Ames, Iowa 50011, USA.
[2] Department of Mechanical Engineering, Iowa State University, Ames, Iowa 50011, USA. Correspondence and requests for materials should be addressed to V.I.L. (vlevitas@iastate.edu).

1

Numerous melting-related phenomena represent fundamental material problems and are currently under intense experimental and theoretical study. They include surface premelting and melting below the thermodynamic melting temperature θ_e, caused by reduction in surface energy and leading to appearance of a molten, nanometer-thick layer[1,2]; reduction in melting temperature θ_m with reduction of the particle radius R down to nanoscale[3,4]; melting of particles with radii comparable to and smaller than the equilibrium solid–liquid interface width δ_e, which is a few nm[3,5]; and overheating above θ_e during very fast heating[6,7]. All of these phenomena allow one to determine the properties of solid and liquid deeply in the region of their metastability and even complete instability (that is, above the solid instability temperature θ_i or below the melt instability temperature θ_c, see Supplementary Fig. S1), and to study intermediate states, various scale effects and non-equilibrium thermodynamic and kinetic properties. These studies also have important applied aspects, for example, for combustion of Al nanoparticles[8], which are the most known representatives of nanoenergetic materials. However, a consistent theoretical framework for the description of the above phenomena is lacking. The sharp-interface approach[9] (SIA) is not justified for the above problems. Although there are important molecular dynamics (MD) studies[5,6,10], we focus on the continuum phase-field approach (PFA), which allows consideration of larger spatial and time scales and operates explicitly with thermodynamic and kinetic parameters determined at the macroscale (see Supplementary Discussion). When mechanics is taken into account, a basic problem of the description of finite-width, solid–liquid interface appears. Traditionally, solids and liquids are described in completely different continuum mechanical frameworks (for example, solids are described in undeformed states, whereas liquids are described in a deformed state), which sophisticates the description of intermediate state. Some works consider solid as a very viscous liquid[13], that is, neglect elastic shear modulus μ. Such a liquid–liquid interface is incoherent and does not generate internal elastic stresses, similar to sharp interface (Fig. 1). Alternatively[14], solid–melt interface is considered as a coherent interface (Fig. 1), in which shear modulus varies from that for solid to zero, and this results in generation of internal elastic stresses at the interface. When particle size is comparable to or smaller than the interface width, a coherent interface is the only reasonable choice. Although this model is supposed to be more precise, the surface tension in it is not consistent with sharp-interface limit, even if $\mu = 0$. Also, even for liquid–liquid interface, expression for surface tension in PFA differs by a hydrostatic pressure from that in SIA[11–13]. This is a fundamental thermodynamic inconsistency, which is especially important for nanoscale interface radii.

Surface premelting and melting were studied using PFA[15–17] without involving mechanics. However, the employed equation for surface energy, $\gamma(\eta) = a + b\eta^2$, did not allow a homogeneous solution for solid ($\eta = 1$) (Fig. 2), exhibiting a surface disordered structure even below melt instability temperature θ_c, when the energy minimum corresponding to melt does not exist. Such an inconsistency also exhibits itself in unphysical regions in the phase diagram[15].

The goal of this paper is to develop a unified PFA coupled to mechanics and reveal the non-trivial features of the above melt-related phenomena. Thus, a model with coherent solid–melt interface is developed (see Fig. 1), in which shear modulus μ varies from that for solid to zero, and this results in generation of internal elastic stresses at the interface. Thermodynamic potential in this model results in surface-tension stresses consistent with the SIA, in contrast to known models with incoherent interface (for which $\mu = 0$)[11–13] and coherent interface[14]. Also, the necessity of introducing a non-spherical transformation strain, which, in addition to volumetric expansion during melting, describes change in shape, is demonstrated. Our model resolves fundamental thermodynamic inconsistency and includes more advanced mechanics, which is especially important
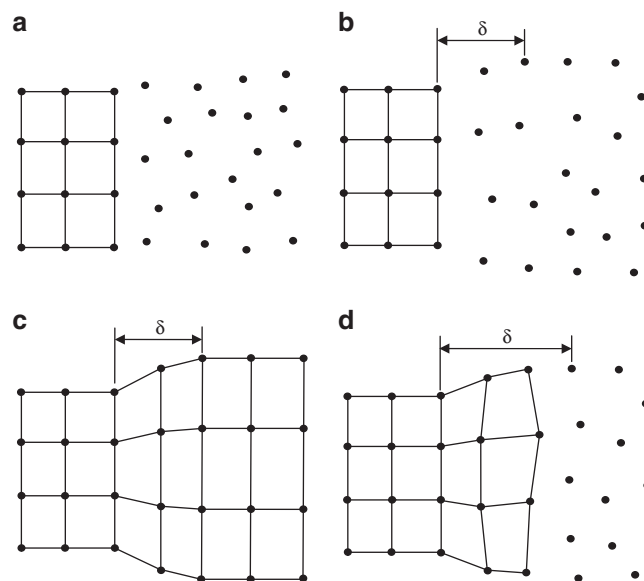
Figure 1 | Different types of interfaces between solid and molten phases.
(**a**) Traditional sharp incoherent solid–melt interface, which does not generate internal elastic stresses. (**b**) Incoherent, finite-width, solid–melt interface with zero shear modulus $\mu = 0$ that does not generate internal elastic stresses. (**c**) Coherent finite-width interface between two solid phases. Continuity of crystal lattice across the interface along with a change in the size of one of the lattices during transformation (due to transformation strain tensor ε_t) generates internal elastic stresses. (**d**) Coherent, finite-width, solid–melt interface with non-zero shear modulus $\mu \neq 0$ that generates internal elastic stresses.

for nanoparticles. Also, a model for surface energy that varies during melting is developed, which resolves the aforementioned non-physical effects in existing models[15–17] and adds mechanics to them. It is demonstrated that our model describes well experimental data on the width of the molten layer versus temperature for the Al plane surface, and then it is applied to surface-induced premelting and barrierless melt nucleation for nanoparticles. It also describes well experimental data on θ_m versus R, even better than MD simulations[5]. Then, non-equilibrium and small-scale regimes were treated, that is, interface profile, width, energy and velocity have been determined and analysed versus R, interface position r_i, and large overheating and heating rates $\hbar$. Thus, the derived analytical expression for interface velocity v describes well simulation results well outside an expected range, namely, even for $\theta > \theta_i$, $\hbar$ up to $10^{13}\,\mathrm{K\,s^{-1}}$, and $r_i \geq 2\,\delta_e$. It also describes well the effect of large compressive and tensile pressure. Homogeneous melt nucleation competes for $\hbar = 10^{13}\,\mathrm{K\,s^{-1}}$ with interface propagation. For $R = 1$ and $3\,\mathrm{nm}$, premelting occurs in the entire particle rather than at the surface only. Allowing for mechanics increases the melting temperature by $70\,\mathrm{K}$ for $R = 1\,\mathrm{nm}$ particle due to pressure induced by surface tension. For $R \leq 1.5\,\mathrm{nm}$, $\theta_m < \theta_c$, that is, the particle melts more than $200\,\mathrm{K}$ below θ_e, while there is no local energy minimum corresponding to melt. While for a liquid–liquid interface our calculations reproduce the Laplace relationship for jump in radial stresses $\Delta\sigma_r$, for coherent solid–melt interface, $\Delta\sigma_r$ does not follow the Laplace relationship and even may possess the opposite sign, causing tension in the solid core instead of compression. Interface energy varies in a non-trivial way for $r_i \leq 4\delta_e \simeq 12\,\mathrm{nm}$ with decreasing r_i, increasing for $\theta > \theta_e$ and decreasing for $\theta < \theta_e$; this is opposite to the behaviour for $r_i > 12\,\mathrm{nm}$.

Results

Theory. We designate contractions of tensors $\boldsymbol{A} = \{A_{ij}\}$ and $\boldsymbol{B} = \{B_{ji}\}$ over one and two indices as $\boldsymbol{A} \cdot \boldsymbol{B} = \{A_{ij} B_{jk}\}$ and $\boldsymbol{A} : \boldsymbol{B} = A_{ij} B_{ji}$,
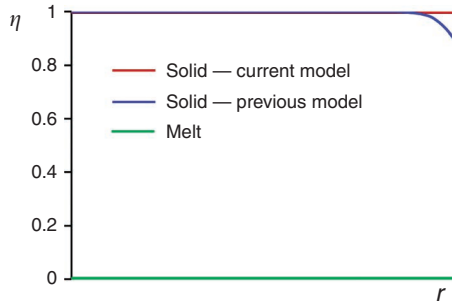
Figure 2 | Stationary solutions for Ginzburg–Landau equation with different models for surface energy. Previous models[15–17] (blue line) did not allow a homogeneous solution for the solid ($\eta = 1$), exhibiting a surface disordered structure at any temperature. Our model equation (8) (red line) is developed using the condition that it allows a homogeneous solution for the solid. The green line represents melt ($\eta = 0$).

respectively. The subscript * means symmetrization; the subscripts or superscripts e, θ and t are for elastic, thermal and transformational contributions to strain and energy; I is the unit tensor; $\Delta A = A_s - A_m$ for any property A, with subscripts s and m denoting solid and melt, respectively; $\overset{o}{\nabla}$ and ∇ are the gradient operators in the undeformed and deformed states; and $\otimes$ designates a dyadic product.

To develop a unified approach to solid and liquid, we will consider liquid as the limit case of isotropic viscoelastic solid with $\mu = 0$. For simplicity, viscosity is neglected, isothermal processes are considered and shear strain is small. However, even if volumetric strain ε_0 is small, in order to reproduce surface tension one has to use fully large-strain formulation (see below). We will modify our recently developed theory of martensitic transformations in solids[18,19] to describe melting. The Helmholtz free energy per unit undeformed volume of solid $\psi = \psi(\varepsilon, \eta, \nabla\eta, \theta)$, in which ε is the strain tensor and η is the order parameter that varies from 1 in solid to 0 in melt. Using an irreversible thermodynamic procedure based on the application of the first and second laws of thermodynamics to the system with energy depending on the gradient of the order parameter (see ref. 12 and references in it) and assuming linear relation between thermodynamic force and flux, one obtains expression for the stress tensor σ and the Ginzburg–Landau (GL) equation

$$\sigma = \frac{\partial\psi}{\partial\varepsilon} - J^{-1}\left(\nabla\eta \otimes \frac{\partial\psi}{\partial\nabla\eta}\right)_*,$$

$$\frac{1}{\chi}\frac{\partial\eta}{\partial t} = -J^{-1}\frac{\partial\psi}{\partial\eta}\Big|_\varepsilon + \nabla\cdot\left(J^{-1}\frac{\partial\psi}{\partial\nabla\eta}\right), \quad J = \frac{\rho_0}{\rho} = 1 + \varepsilon_0, \tag{1}$$

in which ρ_0 and ρ are the mass densities in the non-deformed and deformed states, χ is the kinetic coefficient, and $\varepsilon = \text{const}$ while evaluating $\partial\psi/\partial\eta$. The kinematics relationship between displacement u and strain $\varepsilon = 1/3\varepsilon_0 I + e$, decomposition of ε and the equilibrium equation are given by

$$\varepsilon = (\overset{o}{\nabla}u)_*, \quad \varepsilon = \varepsilon_e + \varepsilon_t + \varepsilon_\theta, \quad \nabla\cdot\sigma = 0, \tag{2}$$

in which e is the deviatoric strain. Energies and strains are defined as follows:

$$\psi = \psi^e(\varepsilon_0, e, \eta, \theta) + J\breve\psi^\theta + \psi^\theta + J\psi^\nabla;$$

$$\psi^e = 0.5(K_m + \Delta K\phi(\eta))\varepsilon_{0e}^2 + 0.5\mu\phi(\eta)e_e : e_e; \tag{3}$$

$$\psi^\theta = H(\theta/\theta_e - 1)\phi(\eta); \quad \breve\psi^\theta = A\eta^2(1-\eta)^2;$$

$$\psi^\nabla = 0.5\beta|\nabla\eta|^2; \quad A := 3H(1 - \theta_c/\theta_e);$$

$$\varepsilon_t = \overline\varepsilon_t(1 - \phi(\eta)); \quad \varepsilon_\theta = (\alpha_m + \Delta\alpha\phi(\eta))(\theta - \theta_e))I; \quad \phi(\eta) = \eta^2(3 - 2\eta). \tag{4}$$

Here K is the bulk modulus, β and α are the gradient energy and linear thermal expansion coefficients, H is the heat of fusion, $\breve\psi^\theta$ is the double-well energy, and $\overline\varepsilon_t$ is the transformation strain that transforms the elemental volume of solid to melt under $\sigma = 0$. While for martensitic phase transformations $\overline\varepsilon_t$ is a tensor connecting two crystal lattices, for melting it is always pure volumetric strain, $\overline\varepsilon_t = 1/3\varepsilon_{0t}I$ [9,11–14]. We will show that the usual assumption causes very high internal stresses and elastic energy within the interface, which suppresses melt nucleation and contradicts with the experiment. Development of a complete theory for $\overline\varepsilon_t$ is not a goal of this paper, but we consider an alternative expression for uniaxial $\overline\varepsilon_t = \varepsilon_{0t}k \otimes k$, in which $k = \nabla\eta/|\nabla\eta|$ is the unit normal to the interface. In this case, the component of transformation strain along the interface is absent, which minimizes internal stresses and their energy. Then equation (1) looks like

$$\sigma = \sigma_e + \sigma_{st}; \quad \sigma_{st} = (\psi^\nabla + \breve\psi^\theta)I - \beta\nabla\eta \otimes \nabla\eta; \tag{5}$$

$$\sigma_e = (K_m + \Delta K\phi(\eta))\varepsilon_{0e} + \mu\phi(\eta)e_e; \tag{6}$$

$$\frac{1}{\chi}\frac{\partial\eta}{\partial t} = \beta\nabla^2\eta - 6J^{-1}[H\left(\frac{\theta}{\theta_e} - 1\right) + \sigma^e\varepsilon_{0t} - 3p_e\Delta\alpha(\theta - \theta_e)$$

$$+ \frac{1}{2}\Delta K\varepsilon_{0e}^2 + \frac{1}{2}\mu e_e : e_e]\eta(1 - \eta)$$

$$- 4A\eta(1-\eta)(0.5 - \eta); \quad 3p_e := \sigma_e : I, \tag{7}$$

in which σ_e and σ_{st} are the elastic stress and surface tension, $\sigma^e = p_e$ for volumetric transformation strain and $\sigma^e = k\cdot\sigma_e\cdot k$ for uniaxial transformation strain. For a phase-equilibrium condition in the stress-free case, $(\beta/2)|\nabla\eta|^2 = \breve\psi^\theta$ (ref. 20), and we have $\sigma_{st} = \beta|\nabla\eta|^2(I - k\otimes k)$, that is, it represents two equal normal stresses along the interface. Thus, σ_{st} is consistent with the SIA, unlike previous approaches[11–14], which resolves a long-standing problem in PFA for melting.

In contrast to previous works on melting and other transformations in solids[14,18], the gradient operator ∇ with respect to the deformed state was used, and the finite-strain factor J was included in the proper places. Although use of ∇ is natural for liquids[11–13], this is not the case for solids. One of the unexpected points is that even for small strains, one cannot assume that $J \simeq 1$ and $\nabla \simeq \overset{o}{\nabla}$, because this leads to zero surface tension. The same thermodynamic procedure[19] that led to equation (1) also results in the boundary conditions

$$J\frac{\partial\psi}{\partial\nabla\eta}\cdot n = \beta\nabla\eta\cdot n = -\frac{d\gamma}{d\eta}, \quad \sigma_n = \frac{2\gamma(\eta)}{R} + \overline p, \tag{8}$$

in which n is the unit normal to the boundary, σ_n is the normal to interface stress, $1/R$ is the mean curvature and $\overline p$ is the external pressure. Equation (8) represents a generalization for the 3-D case and coupling with mechanics of known condition[15,16]. We require the following properties of the surface energy: $\gamma(0) = \gamma_l$; $\gamma(1) = \gamma_s$; $d\gamma(0)/d\eta = d\gamma(1)/d\eta = 0$. The last equation guarantees that homogeneous melt ($\eta = 0$) and solid ($\eta = 1$) satisfy equation (8) and removes contradiction in the known papers[15,16] (see Fig. 2). These properties are met for polynomial $\gamma(\eta) = \gamma_l + \Delta\gamma(a\eta^2 + (4 - 2a)\eta^3 + (a-3)\eta^4)$ of the lowest degree with a parameter a. One can demonstrate that a criterion of barrierless surface-induced melt nucleation is consistent with a sharp-interface condition, $\Delta\gamma > \gamma_{s-l}$, when $a = 3$.

Then $\gamma(\eta) = \gamma_1 + \Delta\gamma\phi(\eta)$. If surface energy does not change during melting, then $\gamma = $ const and equation (8) reduces to traditional boundary condition $\nabla\eta \cdot \boldsymbol{n} = 0$.

We focus on Al nanoparticles; material parameters are given in Supplementary Discussion. In particular, $\theta_e = 933.67$ K, $\theta_c = 0.8\theta_e = 746.9$ K and $\theta_i = 1.2\theta_e = 1120.4$ K, $\delta_e = 2.97$ nm. Note that all material parameters have been obtained for a macroscopic sample with no fitting parameters left. None of our developments (coherent interface with uniaxial transformation strain, expressions for free energy that result in correct expression for surface tension, and expression for surface energy) requires additional material parameters. First, homogeneous heating of particles of radius R was considered and stationary solutions were found for each temperature. The thickness h of pre-molten and completely molten surface layer (determined by an interphase radius r_i, that is, by point with $\eta = 0.5$) have been plotted versus $\theta_e - \theta$ (Fig. 3). At melting temperature, θ_m, the stationary, two-phase solution ceases to exist and interface propagates to the centre.

Size dependence of melting temperature. In Figure 4, the lowest curve is for GL equation only, that is, for neglected mechanics. Below radius $R^* = 6.12$ nm, results for volumetric $\boldsymbol{\varepsilon}_t$ give slightly lower θ_m
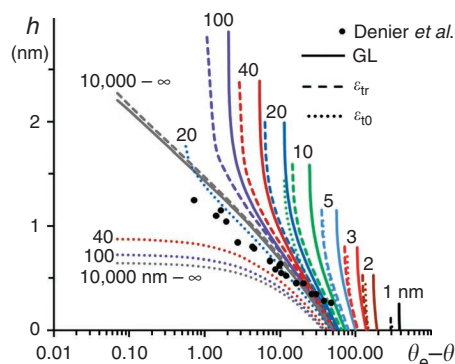

Figure 3 | Thickness of molten surface layer versus temperature for different particle radii. Each colour represents a particle radius shown in nm near the curves. Solid lines are results of the GL model without mechanics. Dotted and dashed lines are obtained for coupled GL and mechanics model with volumetric and uniaxial transformation strains, respectively. Black dots are experimental data[1] obtained using medium-energy ion scattering. Experimental points for a plane surface are close to the calculations for infinite radius for GL and coupled models with uniaxial transformation strain. All curves, excluding those interrupted at 0.1 K, are ended at the melting temperature.
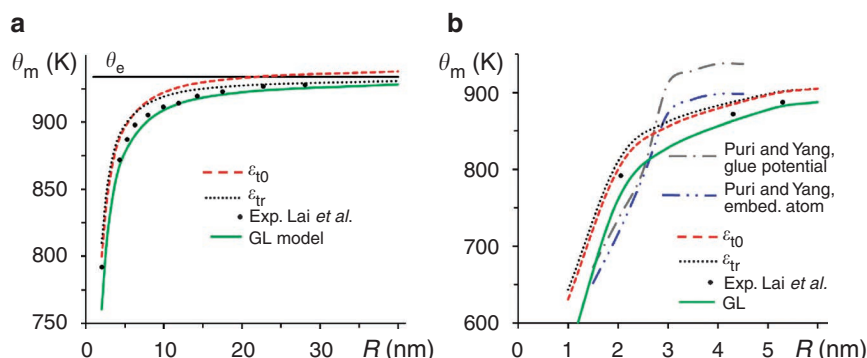
and are closer to the experimental points, whereas for $R > R^*$ results for uniaxial $\boldsymbol{\varepsilon}_t$ are much lower. For $R > 21.2$ nm and volumetric $\boldsymbol{\varepsilon}_t$, $\theta_m > \theta_e$. This is in contrast to the experiments for flat interface, for which $\theta_m = \theta_e$. That is why uniaxial transformation strain was used, in contrast to known models[11–13]. For neglected mechanics and for uniaxial $\boldsymbol{\varepsilon}_t$, melting temperature tends to θ_e for infinite radius. Experimental points are between curves with neglected mechanics and for uniaxial $\boldsymbol{\varepsilon}_t$ for $R > R^*$ and for volumetric $\boldsymbol{\varepsilon}_t$ for $R < R^*$. Coupling with mechanics for 2–3 nm particles increases the melting temperature by 30–40 K (see also Fig. 5) and makes it closer to the experiments. Surprisingly, our results are in better correspondence with experiments than known MD approaches (Fig. 4b). Thus, we can conclude that the model of coherent solid–melt interface has good potential for the description of experiments; traditional volumetric $\boldsymbol{\varepsilon}_t$ is not adequate for large particles, that is, there is interface restructuring, driven by the internal stress relaxation, and a thermodynamic and kinetic theory for $\boldsymbol{e}_t$ should be developed.

Surface premelting and melting. As shown in Figure 3, for a plane interface ($R \rightarrow \infty$), plots for thickness of the molten layer versus θ for GL and uniaxial $\boldsymbol{\varepsilon}_t$ almost coincide and are very close to experimental points, which justifies the validity of our model for surface energy. Results for volumetric $\boldsymbol{\varepsilon}_t$ are inconsistent with experiments. For nanoparticles, $h(\theta)$ plots consist of two parts: an almost straight line with small slope at high temperature with transition to an almost vertical line for temperatures close to θ_m. The maximum thickness of the molten layer is very close for the GL model and the model with uniaxial $\boldsymbol{\varepsilon}_t$. Although curves for these models look also close, for some temperatures the difference in thickness is a factor of 2 or larger. For $R \leq 5$ nm, curves for volumetric and uniaxial $\boldsymbol{\varepsilon}_t$ are very close.

Stationary distributions of interface profiles $\phi(\eta)$ (note that $\phi(\eta)$ rather than η describes the variation of all properties, see equation (1)) in particles of $R = 1$ and 3 nm are presented in Figure 5. For all cases, the complete liquid phase ($\eta = 0$) is not reached. For 1 and 3 nm, stationary premelting (that is, $\phi(\eta) < 1$) occurs in the entire particle rather than at the surface only. Allowing for mechanics increases the melting temperature by 70 K for the $R = 1$ nm particle, mostly due to pressure induced by surface tension. Note that for $R < 1.5$ nm, one has $\theta_m < \theta_c$, that is, the particle melts even when bulk melt is unstable.

Surface tension. Distributions of radial stresses along r are shown in Figure 6. When internal elastic stresses can be neglected (for equal thermoelastic properties of phases and $\mu = 0$, that is, for liquid–liquid transformation, or for $\boldsymbol{\varepsilon}_t = 0$), our calculations at θ_e reproduce the Laplace relationship for jump in radial stresses $\Delta\sigma_r = -2\gamma_{s-l}/r_i$ within an error of 0.14% for $r_i > 11$ nm and 1.03% at $r_i = 5$ nm. For actual solid–
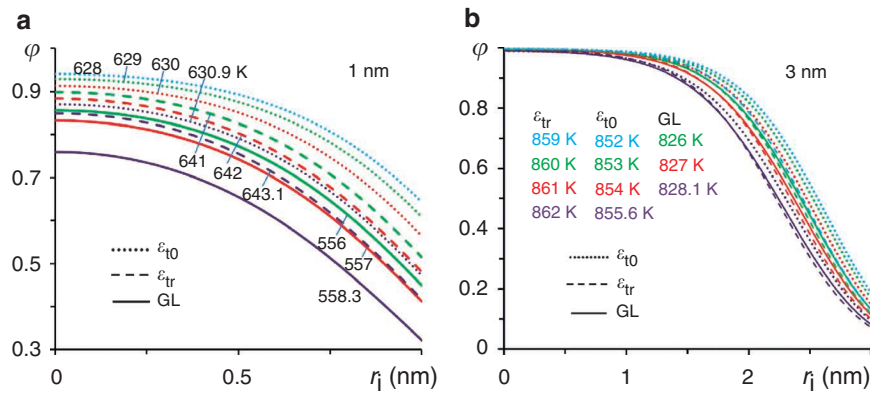

Figure 4 | Melting temperature of Al versus particle radius. (a) Curves are calculated using three models: GL equations only (GL, green line), GL equation coupled to mechanics with volumetric (ε_{t0}) (red line) and uniaxial (ε_{tr}) (black dotted line) transformation strain. Dots are experimental data from Lai et al.[3] obtained using thin-film differential scanning calorimetry. The horizontal line is the equilibrium temperature (the same curve designations are used in **b**). **(b)** Molecular dynamics results are added for particles with radii in the 1–6 nm range. Gray and blue lines are MD results[5] using glue and embedded atom potentials, respectively.

Figure 5 | Stationary interface profiles $\phi(\eta)$ for Al particles for different temperatures. (**a**) $R = 1$ nm; (**b**) $R = 3$ nm. Solid lines are the results obtained with the GL model. Dotted and dashed lines are obtained using coupled GL and mechanics models with volumetric and uniaxial transformation strains, respectively. Different temperatures are considered for each model, which are designated on the graphs. The lowest curve for each model corresponds to the melting temperature.
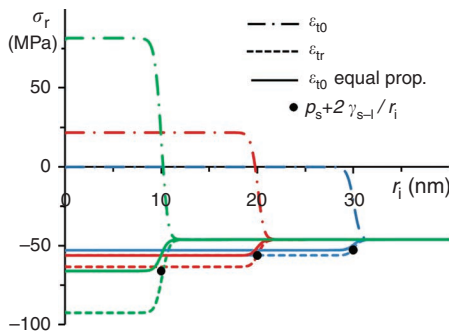

Figure 6 | Distribution of radial stresses for three interface positions. The blue line corresponds to the interface radius at 30 nm, the red at 20 nm, and the green at 10 nm. Distributions are calculated at θ_e using models with volumetric (ε_{t0}) (dotted line) and uniaxial (ε_{tr}) (dashed line) transformation strains, as well as with equal thermoelastic properties of solid and melt (solid line), that is, for liquid–liquid transformation. Dots designate pressures in melt $p_s + 2\gamma_{s-l}/r_i$ based on the Laplace equation that coincides with results of calculations for equal thermoelastic properties of the solid and melt.

Figure 7 | Non-equilibrium interface energy γ_{s-l}^n versus interface radius for different temperatures. Results are obtained for both volumetric and uniaxial transformation strains, and practically coincide. At the position of $r_i = 10$ nm, curves from top to bottom correspond to temperatures of $1.2\theta_e$, $1.1\theta_e$, θ_e, $0.9\theta_e$ and $0.8\theta_e$. A crossover in temperature dependence of interface energy for radii below 20 nm is evident.

melt properties and volumetric ε_t, $\Delta\sigma_r$ does not follow the Laplace relationship and even possesses the opposite sign, causing tension in the solid core (Fig. 6). For uniaxial ε_t, $\Delta\sigma_r = -k2\gamma_{s-l}/r_i$ with $k > 1$.

Interface profile and energy. For plane interface, $\theta = \theta_e$, and neglected mechanics, the GL equation allows analytical solution for an equilibrium interface:

$$\eta_e = [1 + \exp(5.54x/\delta_e)]^{-1}; \quad \delta_e = 5.54\sqrt{\beta/(2A)}; \quad \gamma_{s-l} = \sqrt{\beta A/18},$$
(9)

where the interface width is $\delta = |r_1 - r_s|$ and r_1 and r_s are determined from the conditions $\phi(\eta) = 0.01$ and 0.99, respectively. Surface energy in non-equilibrium state γ_{s-l}^n is defined as an excess energy with respect to solid (where $0.5 < \eta \leq 1$) and liquid (where $0 \leq \eta \leq 0.5$):

$$\gamma_{s-l}^n = \left(\int_0^{r_i} (\rho\psi - \rho_s\psi_s)r^2 dr + \int_{r_i}^{R-h} (\rho\psi - \rho_l\psi_l)r^2 dr \right)/r_i^2. \quad (10)$$

With neglected mechanics, interface width is described by equation (9) within 2.5% error for $r_i \geq 2\delta_e$ and $\theta \leq 1.25\theta_e$, that is, even above θ_i. For $r_i = 2$ nm, $\delta = 3.99$ nm $= 1.34\delta_e$. Mechanics slightly ($<1\%$) increases the width for $\theta = \theta_e$, but this difference grows with increasing temperature; for example, $\delta = 3.03$ and 3.06 nm for $r_i = 30$ nm, $\theta = 1.2\theta_e$ and $1.25\theta_e$, respectively. Still, the interface profile differs
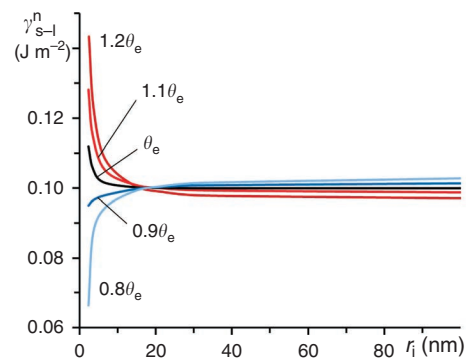
from equation (9) within $\Delta\phi = 0.03$ error for $r_i \geq \delta_e/2$ and $\theta \leq \theta_i$. Interface energy γ_{s-l}^n versus interface radius for different temperatures is shown in Figure 7. For equilibrium temperature, interface energy starts growing for $r_i < 10$ nm and maximum deviation from $\gamma_{s-l} = 0.1$ J m^{-2} is 11.2% for the smallest $r_i = 2.41$ nm, for which full interface exists. For $r_i > 20$ nm expected decrease in γ_{s-l}^n with growing temperature is observed. For $r_i < 20$ nm, unexpectedly the opposite relation is found, which means change in sign of the interface entropy. Note that for $r_i > 4\delta_e \simeq 12$ nm, deviation of γ_{s-l}^n from γ_{s-l} does not exceed 3% in the entire temperature range $\theta_c < \theta < \theta_i$, which is well below the inaccuracy of experimental data for interface energy.

Interface velocity. When internal stresses inside an interface are neglected, the following linear relationship is obtained for $r_i \gg \delta_e$ between interface velocity v_0 and the thermodynamic force for interface propagation per unit deformed volume of solid X:

$$v_0 = 6X\chi\sqrt{\beta\rho_m/(2A\rho_s)},$$

$$X = \frac{\rho_s}{\rho_{0s}} H\left(1 - \frac{\theta}{\theta_e}\right) + p_m\left(\frac{\rho_s}{\rho_m} - 1\right) - \frac{1}{2}\left(\frac{p_m^2}{K_m} - \frac{p_s^2}{K_s}\right) + \frac{2\gamma_{s-l}}{r_i}. \quad (11)$$

It can be seen from Figure 8 that equation (11) describes well (error $\leq 3\%$) results of our simulations even for $r_i > 2\delta_e$ for neglected internal stresses and for heating rates as high as 10^{13} K s^{-1}. Owing to
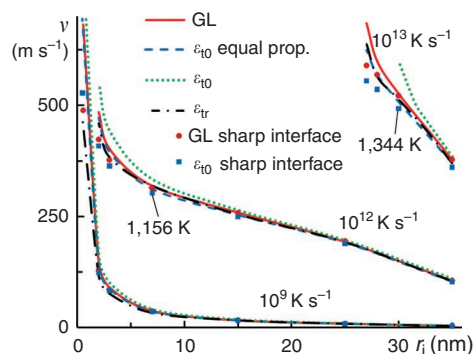
Figure 8 | Interface velocity versus position for three heating rates.
The heating rate is $10^9\,\mathrm{K\,s^{-1}}$ at the bottom, $10^{12}\,\mathrm{K\,s^{-1}}$ in the middle, and
$10^{13}\,\mathrm{K\,s^{-1}}$ at the top. Curves correspond to PFA with different models (red
line for GL model, green and black lines for models with volumetric and
uniaxial transformation strains, respectively, and blue line for volumetric
transformation strain with equal solid and melt properties). Points
correspond to SIA, namely, to equation (11).

small particle size, homogeneous temperature is assumed; see the
analytical justification in ref. 8. The temperature at some points
in Figure 8 significantly exceeds the instability temperature θ_i and
reaches 1344 K for $10^{13}\,\mathrm{K\,s^{-1}}$; that is why interface does not reach
the centre of the particle, because homogeneous reduction of η in
the central part completes melting faster. Even for high compres-
sive and tensile pressures, equation (11) works well when internal
stresses are negligible: for external pressure $p = 4\,\mathrm{GPa}$ and $\theta = 1225\,\mathrm{K}$
deviations from simulations for $r_i = 30$ and $20\,\mathrm{nm}$ are within 2.14%,
and for $p = -4\,\mathrm{GPa}$ and $\theta = 750\,\mathrm{K}$ it is within 1.05%. Velocities for
volumetric ε_t are higher, and for uniaxial ε_t they are lower than for
the case with $\mu = 0$.

Discussion

Note that the SIA[21] to melting/solidification at the nanoscale, which
includes surface-induced melting and coupled to mechanics, can
be applied to our problems down to some radius, which is to be
determined by comparison with PFA. However, when the interface
region is a significant part of the particle, PFA is more precise and
does not require any adjustments. In contrast, SIA should incorpo-
rate the size dependence of surface melting (Fig. 3), size and tem-
perature dependence of surface energy (Fig. 7), and surface stresses
not equal to surface tension (Fig. 6). To summarize, an advanced
phase-field approach to premelting and melting coupled to mechan-
ics is developed. It is applied to study melting deeply in the region
of metastability and complete instability of solid and melt, interme-
diate states at the surface and in few nm-size particles, scale effect,
and non-equilibrium thermodynamic and kinetic properties. The
importance of mechanics effects (even without external pressure)
is elucidated. Crossover in temperature dependence of the interface
energy for radii below 20 nm and violation of the Laplace relation-
ship for the jump in pressure is obtained. Conceptual validity of the
coherent solid melt is proven and necessity for its further develop-
ment, namely, formulation of the evolution equation for the devia-
toric part of ε_t, is demonstrated.

Methods
**The finite element method code COMSOL Multiphysics was utilized to solve
coupled equations (2)–(8).** Quadratic Lagrangian elements are used for both
the mechanical and GL differential equations. In all, 15–30 elements per interface
width and an adaptive time step with a minimum of 1,000 time steps for a typical
non-stationary problem are used. To check the model, interface profiles are com-
pared with analytical results for plane interface at equilibrium temperature[22]. Even

with an interface radius of 30 nm, difference between planar analytical solution and
COMSOL GL result is less than 0.1%. Also, the solid–liquid interface energy in Al
practically coincides with its analytical value of $0.1\,\mathrm{J\,m^{-2}}$, see Figure 7.

References

1. Denier van der Gon, A. W., Smith, R. J., Gay, J. M., O'Connor, D. J. & van der
   Veen, J. F. Melting of Al surfaces. *Surf. Sci.* **227,** 143–149 (1990).
2. Henson, B. F. & Robinson, J. M. Dependence of quasiliquid thickness on the
   liquid activity: a bulk thermodynamic theory of the interface. *Phys. Rev. Lett.*
   92, 246107 (2004).
3. Lai, S. L., Carlsson, J. R. A. & Allen, L. H. Melting point depression of Al
   clusters generated during the early stages of film growth: nanocalorimetry
   measurements. *Appl. Phys. Lett.* **72,** 1098–1100 (1998).
4. Levitas, V. I., Pantoya, M., Chauhan, G. & Rivero, I. Effect of the alumina shell
   on the melting temperature depression for nano-aluminum particles. *J. Phys.
   Chem. C* **113,** 14088–14096 (2009).
5. Puri, P. & Yang, V. Effect of particle size on melting of aluminum at nano scales.
   J. Phys. Chem. C **111,** 11776–11783 (2007).
6. Ivanov, D. S. & Zhigilei, L. V. Combined atomistic-continuum modeling of
   short pulse laser melting and disintegration of metal films. *Phys. Rev. B* **68,**
   064114 (2003).
7. Iglev, H., Schmeisser, M., Simeonidis, K., Thaller, A. & Laubereau, A. Ultrafast
   superheating and melting of bulk ice. *Nature* **439,** 183–186 (2006).
8. Levitas, V. I., Asay, B. W., Son, S. F. & Pantoya, M. Mechanochemical
   mechanism for fast reaction of metastable intermolecular composites based on
   dispersion of liquid metal. *J. Appl. Phys.* **101,** 083524 (2007).
9. Grinfeld, M. A. *Thermodynamic Methods in the Theory of Heterogeneous
   Systems* (Longman, 1991).
10. Delogu, F. Mechanistic aspects of homogeneous and heterogeneous melting
    processes. *J. Phys. Chem. B* **110,** 12645–12652 (2006).
11. Lowengrub, J. & Truskinovsky, L. Quasi-incompressible Cahn-Hilliard
    fluids and topological transitions. *Proc. R. Soc. London A* **454,** 2617–
    2654 (1998).
12. Anderson, D. M., McFadden, G. B. & Wheeler, A. A. A phase-field model of
    solidification with convection. *Physica D* **135,** 175–194 (2000).
13. Anderson, D. M., McFadden, G. B. & Wheeler, A. A. A phase-field model
    with convection: sharp-interface asymptotics. *Physica D* **151,** 305–331
    (2001).
14. Slutsker, J., Thornton, K., Roytburd, A. L., Warren, J. A. & McFadden, G. B.
    Phase field modeling of solidification under stress. *Phys. Rev. B* **74,** 014103
    (2006).
15. Pluis, B., Frenkel, D. & Van der Veen, J. F. Surface-induced melting and freezing.
    2. A semiempirical Landau-type model. *Surf. Sci.* **239,** 282–300 (1990).
16. Lipowsky, R. Critical surface phenomena at 1st-order bulk transitions. *Phys.
    Rev. Lett.* **49,** 1575–1578 (1982).
17. Chang, J. & Johnson, E. Surface and bulk melting of small metal clusters. *Philos.
    Mag.* **85,** 3617–3627 (2005).
18. Levitas, V. I., Levin, V. A., Zingerman, K. M. & Freiman, E. I. Displacive phase
    transition at large strains: phase field theory and simulations. *Phys. Rev. Lett.*
    103, 025702 (2009).
19. Levitas, V. I. & Javanbakht, M. Surface tension and energy in multivariant
    martensitic transformations: phase-field theory, simulations, and model of
    coherent interface. *Phys. Rev. Lett.* **105,** 165701 (2010).
20. Levitas, V. I., Preston, D. L. & Lee, D. W. Three-dimensional Landau theory for
    multivariant stress-induced martensitic phase transformations. *Phys. Rev. B* **68,**
    134201 (2003).
21. Hoyt, J. J. Effect of stress on melting and freezing in nanopores. *Phys. Rev. Lett.*
    96, 045702 (2006).
22. Levitas, V. I., Lee, D. W. & Preston, D. L. Interface propagation and microstructure
    evolution in phase field models. *Int. J. Plast.* **26,** 395–422 (2010).

Acknowledgments

Author contributions
V.L. proposed the research and developed theory. K.S. performed the phase field
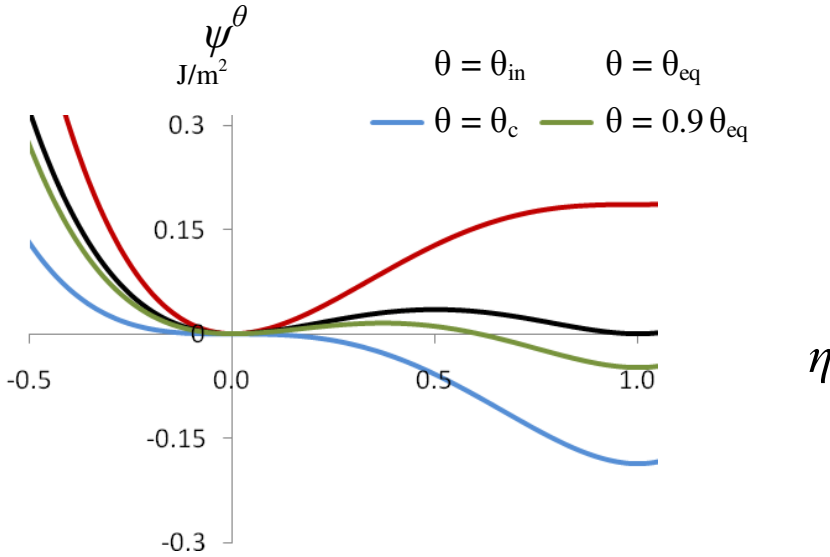simulations.

Additional information

Supplementary Figure

Supplementary Figure S1. Thermal part of the thermodynamic potential ψ^θ vs. order parameter η for different temperatures. At equilibrium temperature θ_c, potential has two equal minima $\eta = 0$ and $\eta = 1$, corresponding to liquid and solid. For lower temperature (for example, $0.9\theta_e$), minimum corresponding to solid reduces (solid is thermodynamically stable), but there is an energy barrier between phases, i.e., liquid is metastable. At and below the melt instability temperature θ_c, the minimum corresponding to liquid disappears and melt is unstable. Similarly, at and above the solid instability temperature θ_i, the minimum corresponding to solid disappears and solid is unstable.

Supplementary Discussion

Short review of existing approaches and problems

There are two main continuum methods of studying melting: the sharp-interface approach[9] (SIA) with jump of thermodynamic parameters across an interface with $\delta = 0$, and the phase-field approach (PFA), in which melting is described by continuous variation of an order parameter η from 1 to 0 across the interface of finite width [11-17]; all other thermodynamics parameters are continuous across an interface as well.

The evolution of η is described by Ginzburg-Landau (GL) or phase-field equation, which represents the linear relationship between $\dot{\eta}$ and conjugate thermodynamic force X. The PFA is more detailed than the SIA but requires more advanced thermodynamic potential that describes intermediate states between solid and liquid in terms of the order parameter η (Supplementary Figure S1) and interface energy in terms of gradient $\nabla\eta$. One of the requirements for PFA is that for the sample size $L/\delta \gg 1$, equations of

PFA should transform to those of SIA. This is, however, not the case in known publications for surface tension, because expressions for surface tension in both approaches differ by a hydrostatic pressure[11-13]. This is a fundamental thermodynamic inconsistency, which is especially important for nanoscale interface radii. In the paper, we find expression for thermodynamic potential for PFA, which results in consistent expression for surface tension, and we derive the kinetic relationship for interface velocity, v, for $L/\delta \gg 1$, i.e., $v_0(X)$.

For nanoparticles and solid-liquid interface radii r_i that are comparable with interface width δ, SIA fails and PFA is the only reliable continuum approach. It is expected that interface energy may depend on the interface radius and that the interface velocity v may deviate from the kinetic relationship $v_0(X)$ obtained for $\bar{r} = r/\delta \gg 1$. SIA also fails when nanoparticles are overheated fast to temperature θ close or even above the crystal lattice instability temperature θ_i, at which energy minimum corresponding to solid disappears (Supplementary Figure S1). One of our goals is to study numerically these non-equilibrium and small-scale regimes, i.e., determine and analyze interface profile, width, energy, and velocity.

Material parameters for aluminum

We will focus on Al nanoparticles and use the following material parameters obtained for macroscopic sample[1,3,8,15]: $H = 933.57 \times 10^6$ J/m^3, $K_m = 41.3 GPa$, $K_s = 71.1 GPa$, $\alpha_m = 4.268 \times 10^{-5}$ K^{-1}, $\alpha_s = 3.032 \times 10^{-5}$ K^{-1}, $\gamma_s = 1.050$ J/m^2, $\Delta\gamma = 0.129$ J/m^2, $\beta = 3.21 \times 10^{-10}$ N, $\chi = 400$ m^2/Ns, $\theta_c/\theta_e = 0.8$ (which leads to $\theta_i/\theta_e = 1.2$, $\theta_c = 746.9K$, and $\theta_i = 1120.4K$). To determine β we used $\gamma_{s-l} = 0.1$ J/m^2 from[3] and Eq.(9), and to determine χ we used interface mobility $1.283 m/(sK)$ obtained with MD simulation (Mendelev, M. private communication, 2010) and Eq.(11), both for plane interface. For such parameters, equilibrium interface thickness $\delta_e = 2.97nm$ (Eq.(9)).

Justification of the model of coherent interface and non-spherical transformation strain for melting

Below, we will show that in the framework of any phase-field theory, which takes into account finite interface width and elasticity, our model of coherent interface and non-spherical transformation strain for melting are straightforward and natural.

First, as in any phase-field theory, we assume continuity of displacements. Second, as in any phase-field theory, we assume that within interface any property varies from the value for solid to that of the melt; these should include shear modulus and transformation strain. Third, with this model and traditional assumption of pure volumetric transformation strain, we obtained large elastic stresses and energy inside the interface, which led to a large deviation of theory from experiments for thickness of the molten layer (Fig. 3) and size dependence of the melting temperature (Fig. 4). And fourth, it is clear that the missing physics is in the relaxation of elastic stresses, i.e., introducing an inelastic deviatoric strain (volumetric transformation strain is completely determined by the ratio of densities of phases). While it is completely unexpected and new for melting, the phase-field approach describes intermediate states

between solid and melt, and the only reasons that transformation strain was accepted to be pure volumetric are the tradition and that the deviatoric part is unknown (in contrast to martensitic transformations). However, unknown does not mean that it is zero. It is clear that one has to develop a thermodynamically consistent kinetic equation for deviatoric part of the transformation strain, but this is a separate and complex problem. Thus, we considered the simplest limit case of uniaxial transformation strain normal to the interface, which minimizes internal stresses along the interface and their energy and does not require additional material parameters.

Since we obtained very reasonable (but not perfect) correspondence with experiments, we concluded in the paper that: the model of coherent solid-melt interface has good potential for the description of experiments; traditional volumetric ε_t is not adequate for large particles, i.e., there is interface restructuring, driven by the internal stress relaxation; and a thermodynamic and kinetic theory for ε_t should be developed.